Observation of Resonances Associated with Stereo and Regio Defects in the Crystalline Regions of Isotactic Polypropylene: Toward a Determination of Morphological Partitioning

D. L. VanderHart*

Polymers Division, National Institute of Standards and Technology, Gaithersburg, Maryland 20899-8544

Rufina G. Alamo

Department of Chemical Engineering, Florida Agricultural Mechanical University−Florida State University, 2525 Pottsdamer Street, Tallahassee, Florida 32310-6046

Marc R. Nyden

Fire Science Division, National Institute of Standards and Technology, Gaithersburg, Maryland 20899

M.-H. Kim

Department of Chemical Engineering, Florida Agricultural Mechanical University−Florida State University, 2525 Pottsdamer street, Tallahassee, Florida 32310-6046

L. Mandelkern

Department of Chemistry, Florida State University, Tallahassee, Florida 32306

Received December 7, 1999; Revised Manuscript Received April 25, 2000

ABSTRACT: We report defect-resonance patterns associated with two kinds of low-concentration defects typically found in metallocene-synthesized isotactic polypropylenes (iPP's). These defects are the simple mrrm stereo defect and the regio 2,1-erythro defect. This work is a critical part of our effort to determine the extent to which various defects, typically found in isotactic polypropylene (iPP) samples, are incorporated into the crystalline regions of this semicrystalline polymer. The relationship between defect concentrations and mechanical (as well as thermal) properties is quite dependent on the extent of incorporation of defects into the crystalline regions. Several melt-crystallized (at a cooling rate of 1 °C/min) iPP samples, whose concentrations of various stereo and regio defects are known from high-resolution NMR, have been examined in the solid state by ^{13}C NMR. Using a method based on differences in the rotating-frame proton relaxation times of the crystalline (CR) and the noncrystalline (NC) regions, signals from the CR and the NC regions are separated. The resulting "CR" spectra, pertaining to the CR regions of the iPP, are examined for distinct resonances associated with such defects; relative integrals associated with these resonances are also determined. Definite defect-resonance patterns associated with both the simple mrrm stereo defect and the regio 2,1-erythro defect have been identified. One of our samples, having a rather low molecular weight, contained a substantial amount of the regio 1,3 defect. The corresponding CR spectrum had no sharper resonances that would indicate the presence of 1,3 defects in the CR lattice. Associated with each type of defect, "*i*", we define a partitioning coefficient, $P_{CR}(i)$, as the ratio of the *i*th-defect concentration in the CR region to the overall *i*th-defect concentration. While we cannot, at this point, be absolutely sure about assignments which ultimately dictate the crucial correspondence between defect populations and defect intensities, we can make arguments or assumptions about this correspondence and then suggest P_{CR} values for the stereo and regio defects. On the basis of the arguments and assumptions made herein, the following values are obtained: P_{CR}(stereo: mrrm) = 0.48 ± 0.06 and P_{CR}(regio: 2,1-erythro) = 0.28 ± 0.08. In principle, partitioning coefficients might depend on both on the crystallization kinetics and the crystal habit. Many of our samples possessed mixed amounts of α- and γ-crystallites. The few indications we have suggest that there is only a weak dependence, if any, on kinetics or crystal habit. The hypothesis is considered that those defects seen in the CR spectrum are highly concentrated at the CR/NC interface. On the basis of a modeling of the experimental proton polarization, including spin diffusion, it is concluded that the defects are not highly concentrated on the CR side of the interface; at the same time, we have no information about the possibility of defect concentration on the NC side of the interface. Finally, one of our samples was an iPP pseudofraction derived from an inhomogeneous Ziegler−Natta polymerization. P_{CR}(stereo) for this sample was lower than for the metallocene iPP's, including one with a similar overall defect concentration. Our results support the notion that the Ziegler−Natta pseudofraction consists of a much more inhomogeneous distribution of defect concentrations per chain than that which typifies metallocene iPP's.

Introduction

The tailoring of polymer properties is an area of wide commercial interest. For a large-volume commercial polymer like isotactic polypropylene (iPP), one can generate a considerable range of properties by introducing "defect structures" into the polymer in varying concentrations, where usually a few percent, or less, of the monomer sites are occupied by defects. These defect structures include stereo-type[1], regio-type,[1] and comonomer-type defects. One of the principal mechanisms by which properties are thus modified involves changes

10.1021/ma992041p CCC: $19.00 © 2000 American Chemical Society
Published on Web 07/21/2000

that occur in the crystalline phase of this semicrystalline polymer. At the level of the unit cell, changes in defect concentrations can alter the level of crystallinity[2] as well as the thickness[3] and melting point[4] of those crystallites. A key piece of information for understanding the role that each kind of defect plays in property modification is the partitioning of defects between the crystalline (CR) and the noncrystalline (NC) regions.

In this paper we will use solid-state NMR to address the question of partitioning. For each type of defect, indexed by the letter '*i*', we will seek to measure what we will call the crystalline partitioning coefficient, $P_{CR}(i)$, which we define to be

$$P_{CR}(i) = [C(i)]_{CR}/[C(i)]_{Ave} \quad (1)$$

where $[C(i)]_{CR}$ is the concentration of the *i*th defect in the CR region and $[C(i)]_{Ave}$ is the sample-average concentration of the *i*th defect. The NMR method[5] we use for isolating the signals from the CR regions of iPP is based on a cross-polarization[6] (CP) method where differences in the rotating frame proton relaxation time, $T_{1\rho}^{H}$, corresponding to the CR and NC regions, allow us to obtain multiple spectra with differently weighted contributions from each type of region. This method involves some assumptions about the morphology and the distribution of defects within each region. We discuss this method in some detail herein and critique the method and the results in terms of the possibility that a high concentration of defects collects at the CR/NC interface.

The advent of metallocene catalysts[7] with their varied structures allows one to select the concentrations of stereo and regio defects in any iPP product via the particular choice of catalyst and polymerization conditions (e.g., temperature). These homogeneous metallocene catalysts produce a more uniform iPP with a narrower molecular weight distribution compared to the iPP materials polymerized using the heterogeneous, Ziegler−Natta-type catalysts which were the principal catalysts in use earlier. The metallocene iPP's, with their more uniform structure, are better materials for investigating partitioning than their heterogeneous Ziegler−Natta counterparts since the latter products likely consist of separate populations of chains,[8] each having different average levels and types of defects. Supposedly these distinct populations arise from differing sites within the heterogeneous catalyst. The materials used in this study are mainly metallocene iPP's with one Ziegler−Natta pseudofraction used for comparison. The highly defective, noncrystallizing chains in the original iPP are largely eliminated in the preparation of the pseudofraction.

Solution-state, high-resolution ^{13}C NMR reveals different patterns of resonances associated with various kinds of defects, and these patterns are well-known for both stereo[1,9,10] and regio[1,11−13] defects. Moreover, from such spectra, $[C(i)]_{Ave}$ values can be obtained. From eq 1, only $[C(i)]_{CR}$ need be obtained from the solid-state spectra in order to determine $P_{CR}(i)$ values.

In solution, defect-free iPP chains give rise to one resonance for each of the three carbons in the repeat unit. If defect-containing iPP chains are observed in solution, it is found that the stereo-type defects give rise to smaller chemical shift differences, relative to the shifts of the perfect chain, than do regio-type defects. That is to say, the stereo defect represents a relatively small perturbation since it retains the head-to-tail sequence; only the pendant methyl group is out of place. In contrast, the regio defect (e.g., a head-to-head addition) is a larger perturbation on the chemical shift since it interrupts the alternation of methylene and methine carbons along the backbone. One might therefore anticipate that with the poorer level of resolution in the solid state, compared to the solution state, one would only have a chance of distinguishing regio-defect (not stereo-defect) resonances from the normal backbone resonances. As will be seen, that expectation is erroneous. Typically, several defect resonances associated with both stereo and regio defects in the CR regions are shifted well away from the main backbone resonances. Ostensibly, the reason for the substantial differences in chemical shift between liquid and CR arises from the fact that when a defect is incorporated, as an isolated defect, into a CR region, it (a) adopts a minimum-energy conformation in its host lattice (so it is not dynamically averaged over many conformations as it is in a liquid) and (b) it is likely that this minimum-energy conformation is *strained* because the defect will not fit into the lattice as easily as a normal, nondefective monomer would (strained bonds produce chemical shift changes[14]).

There are two main crystallographic forms associated with melt-crystallized iPP, namely, the α[15−17] and γ[18,19] forms. We ignore the β[20] form which appears only when crystallization occurs in the presence of a very large temperature gradient or by the use of specific nucleating agents. The individual iPP stems that traverse each crystallite in all three allomorphs are claimed to adopt a 3_1 helical conformation whose helical axis is presumed linear. The α form is usual in the sense that all stem axes are parallel; the γ form is unique in the sense that the crystal is made up of thin layers of stems where the stem axes in the same layer are parallel but in adjacent layers alternate in direction by about 80°.[18,19] Owing to this qualitative difference in the structures of the α and γ crystallites, it seemed to us quite possible that a stem containing a defect would, after rearranging itself into a lowest-energy conformation near the defect, see rather disparate interstem interactions, depending on the allomorph. Thus, the $P_{CR}(i)$ should depend on the particular allomorph. In fact, a hint of this may be offered in the observation[21−23] that often an increase in the number of defects tends to promote a higher fraction of γ crystallites, even though, for a given iPP, that fraction is also dependent on the crystallization temperature.[21]

We intended to investigate the dependence of P_{CR} on allomorph; however, we were somewhat thwarted in our attempts. In principle, the best way to investigate this dependence is to try to crystallize the same material under conditions which maximize either the α or the γ allomorphs. In most cases, these conditions also represented fast versus slow crystallization,[21] where the lattice in the sample with fast crystallization was much more poorly organized, compared to the lattice formed by slower crystallization. As a practical matter, the more poorly organized lattice also had broader lines so that we had more difficulty identifying weak defect resonances in the immediate vicinity of the enormous parent resonances. In addition, fast crystallization also raises the issue of *kinetic trapping of defects*, and if this is important, whether the P_{CR} measured for such a sample has any generality.

For any lattice in which $P_{CR} < 1$ (i.e., there is some discrimination against the incorporation of a defect into

Table 1. iPP Samples, Melt Crystallized at 1 °C/min, with Corresponding Selected Properties[a]

sample	M_w (kg/mol)	M_w/M_n	f_D[b]	T_m (°C)[c]	f_γ[d]	f_C(DSC)[e]	f_C(NMR)[f]
M327-0.42R2	327(15)	2.2(2)	0.0042(2)	?	≈0.02	?	0.73
M200-0.42R2	200(10)	≈2	0.0042(3)	162.5	≈0.02	0.55	0.70
M236-1.17R2	236(12)	≈2	0.0117(10)	156.3	0.35	0.49	0.68
M346-1.0S	346(17)	2.3(2)	0.0112(5)	155.6	0.33	0.49	0.72
M335-2.34S	335(17)	2.3(2)	0.0260(10)	133, 142.8	0.55	0.45	0.66
M9.8-2.80R3	9.8(5)	?	0.0280(38)	121	0.90	0.20	0.66
Z250-0.9S	250(13)	5(1)	0.0086(5)	165.5	≈0	0.57	0.73

[a] The full range of uncertainty, in units of the least significnat digit, is either given in parentheses or defined in the footnotes. [b] Total fraction of monomers occupying defect sites, including both stereo and regio defects. [c] Melting temperature determined by DSC; for M335-2.34S, two melting peaks were observed. Full uncertainty is ±0.5 °C. [d] Mass fraction of the crystalline material present as the γ-allomorph; the balance is the α-allomorph. Full uncertainty is ±0.05. [e] Crystalline mass fraction as determined by DSC using a heat of fusion for the crystal of 502 J per mole of repeating unit. Uncertainties depend on assumptions; reproducibility of measurement is ±0.02. [f] Crystallinity as determined by deconvoluting the NMR 0-ms-SL CPMAS line shape into CR and NC contributions (see text). Corrections have also been made for the different $T_{1\rho}^H$'s in the CR and NC regions as well as for the different CP enhancement factors pertaining to the CR and NC regions; combining these corrections effectively multiplies the NC signal by $^4/_3$ relative to the CR signal in the 0 ms SL spectrum. Uncertainty is hard to estimate since there is a dependence on assumptions made. These measurements use NC line shapes similar to those shown in Figure 1. There is a reduction of about 0.04−0.06 in these values if no negative-going features, such as are seen in Figure 1, are allowed near the maxima of the NC resonances. Reproducibility, using a given set of assumptions, is ±0.03.

the lattice), one can always ask the question whether the incorporation of defects into the lattice is expected on the basis of equilibrium thermodynamics (where the generality of P_{CR} is assured) or whether incorporation of defects is always a kinetic matter (where generality of P_{CR} is an issue). We do not take sides on this question in this presentation; rather, we will content ourselves with trying to determine P_{CR} values for samples that are prepared in a simple, reproducible way, i.e., by cooling at 1 °C/min during crystallization. In this way we try, at least to zeroth order, to put the kinetics on a similar footing for all samples, especially in recognition that the defect concentration will influence the crystallization rate[21] at any given crystallization temperature. For the few cases where we have prepared the same sample in multiple ways, we will watch for variations in the measured defect intensities that might indicate some dependence on allomorph or on kinetics.

The results presented in this paper deal only with stereo and regio defects, not comonomer defects; we will deal with partitioning in the presence of comonomers in separate publications. Furthermore, the results reported herein emphasize the *experimental findings* which include the identification and signal integration of resolvable, additional lines associated with the stereo and regio defects. The results reported here are *incomplete,* as final determinations of P_{CR}, in the sense that we have to make assumptions about how many distinguishable resonances arise from each defect. This is not a trivial issue. We have begun to tackle this problem which involves (a) finding the minimum-energy conformation by doing simulated thermal annealing followed by appropriate minimum-energy calculations for an isolated defect confined in the iPP lattice and then (b) calculating chemical shifts for the carbons at each position along this conformationally altered chain. Very little of this effort to assign resonances will be reported herein since we are actively engaged in but have not completed this effort. We thought it to be of sufficient value to identify patterns associated with defects in the CR regions and to underscore the fact that such defects, while discriminated against, are incorporated into the CR regions to a considerable degree.

Experimental Section

The iPP samples are mainly experimental samples, all but one supplied by companies. Molecular mass and microstructural information are included in Table 1. Sample Z250-0.9S is a pseudofraction obtained from a Ziegler−Natta commercial iPP, and it is the only sample whose constituent ratios were modified in a preliminary processing step. This sample was obtained by dissolving the whole Ziegler−Natta iPP in *p*-xylene (0.2 wt % solution) and letting the polymer crystallize slowly from the solution. This process removes, preferentially, the amorphous fraction present in the commercial polymer. The characterization data listed in Table 2 for Z250-0.9S are obtained from the ^{13}C NMR spectrum of this pseudofraction. Microstructural characterization of these polymers has been performed by solution-state ^{13}C NMR at 7.1 T using 10 mm o.d. sample tubes. Fifteen percent solutions in deuterated tetrachloroethane were used and the spectra obtained at 125 °C. Assignment of resonances to defects is based on published assignments.[1,9−13]

NMR samples, unless otherwise noted, were right-circular cylinders (6 mm o.d. and 12 mm high). These cylinders were machined from larger rods that were, in turn, melt crystallized by (1) melting pellets or powder into an 8 mm i.d. glass tube under vacuum at 190 °C to 200 °C with mild pressure applied to collapse the resulting voids, (2) cooling the polymer in a vacuum, (3) reintroducing an atmosphere of nitrogen gas, (4) sealing the glass tube with the nitrogen gas inside the tube at equilibrium with ambient pressure, and (5) heating the sealed tube to 190−200 °C in a convection oven for about 4 h followed by a cooldown cycle programmed at 1 °C/min down to 35 °C. The sealed glass tube was inserted into a large brass block in the oven during this melt crystallization cycle. While there is a thermal lag associated with the sample being in this block, the significant drop in temperature required to reach crystallization temperatures ensures that during crystallization the temperature ramp seen by the sample is very close to 1 °C/min.

The solid-state ^{13}C NMR experiments were conducted at 2.35 T (25.2 MHz) on a noncommercial spectrometer which uses a noncommercial probe whose rotor and stator are manufactured by Doty Scientific, Inc.[24] All spectra were taken at ambient temperature using a magic angle spinning[25] (MAS) frequency of 4.0 kHz and nutation frequencies associated with the strengths of the ^{13}C and proton radio-frequency fields of 66 and 62 kHz, respectively. The typical period between acquisitions was 5 s, and the usual signal observation window, with high-power proton decoupling, was 140 ms. The NMR method[5] utilized for separating the ^{13}C signals arising from the crystalline (CR) and the noncrystalline (NC) regions of iPP is based on differences in the intrinsic rotating-frame relaxation times, $T_{1\rho}^H$, as well as differences in the ^{13}C line widths, associated with each region. By spin-locking[26] the proton polarization for two different times (0 ms and 6−8 ms) prior to cross-polarizing (for 0.7 ms) from the protons to the ^{13}C nuclei, one obtains a pair of ^{13}C spectra for each sample where each spectrum represents a differently weighted contribution from the CR and NC regions. In particular, as the spin-locking

Table 2. Fractional Defect Populations of Propylene Repeat Units of Various Kinds in the IPP Samples Based on High-Resolution ^{13}C NMR Results; Stereo-Defect Populations Are Expressed as Concentrations of Pentads[x], Deduced from Analysis of the Methyl Region of the IPP Spectra[a]

sample	stereo mmmr[b]	stereo mmrr	stereo mrrm[c]	stereo (mmrm + rrmr)	stereo rmrm	2,1 defect:erythro	2,1 defect:threo	1,3 defect	total defects[d]
M327-0.42R2	0.0002(0)	–	<0.0001		–	0.0041(2)	–	–	0.0042(2)
M200-0.42R2	0.0004(1)	–	<0.0002		–	0.0040(2)	–	–	0.0042(3)
M236-1.17R2	0.0044(4)					0.0095(6)	–	–	0.0117(10)
M346-1.0S	0.0192(5)	0.0157(4)	0.0073(1)	0.0011(1)	0.0002(0)	0.0016(2)	–	–	0.0112(5)
M335-2.34S	0.0386(11)	0.0317(6)	0.0143(4)	0.0065(1)	0.0007(1)	0.0023(1)	0.0030(2)	0.0015(1)	0.0260(10)
M9.8-2.80R3	0.0077(30)	0.0026(26)	≈0.0011[e]			–	–	0.0242(8)	0.0280(38)
Z250-0.86S	0.0172(5)	0.0153(4)	0.0063(4)	0.0039(1)	0.0006(1)	–	–	–	0.0086(5)

[a] Dashes indicate that a resonance pattern was looked for but was too small to measure; a blank cell indicates that this data was not determined. Standard uncertainties, in units of the last significant digit, follow in parentheses. [b] We define our "total stereo-defect concentration" equal to 0.5 times this number. Such a "total" concentration is only total within the narrow definition that a stereo defect, corresponding to a specific dyad sequence, is a single defect so long as the separation between nearest "r" dyads in the sequence is less than 3 "m" dyads. Any such sequence will always have two, and only two, associated mmmr (= rmmm) pentads located at the beginning and end of the stereo-defect sequence. [c] This number is the most accurate estimate of the concentration of the generally most dominant stereo defect. This defect consists of a perfect iPP stereosequence in which a single, isolated repeat unit has its methyl group out of the usual stereochemical order. In principle, sequences such as "mrrmmrrm" or "mrrmrrm" would contribute to the mrrm pentad intensity even though these sequences would not represent the isolated defect just defined; however, the contribution of such sequences to the mrrm pentad intensity is minor[Randall]. [d] This number is 0.5[mmmr] + [2,1-erythro] + [2,1-threo] + [1,3]. [e] Estimated value of 0.44[mmrr], following the measured relationship between [mrrm] and [mmrr] for the other samples.

time increases, the relative NC contribution diminishes. If one takes appropriate linear combinations of spectra with, say, 0 and 7 ms spin-locking times, one can isolate the spectrum of the CR and the NC regions, subject to a few assumptions which we will address in more detail in the Results section. We choose this method for separating CR and NC resonances over an alternative method[27] that is based on differences in ^{13}C longitudinal relaxation time, T_1^C. The reason for our choice is that ^{13}C nuclei at the defect sites may have mobilities and T_1^C's somewhat different from the T_1^C's of the corresponding, neighboring nondefect carbons; hence, one may be inclined to assign such carbons to an inappropriate location. (Also, the faster relaxing methyl carbon in both the CR and the NC region and the accompanying possibilities of $^{13}C-^{13}C$ spin exchange[28] make the CR/NC distinctions in T_1^C smaller for iPP than for a system devoid of methyl groups, e.g., polyethylene.) The big advantage of this method, however, is that the polarization of the dilute defect protons (and, via CP, their counterpart ^{13}C nuclei) track closely the behavior of the polarization of those protons (and ^{13}C nuclei) immediately surrounding the defect site, regardless of possible differences in mobility. Our method also has a disadvantage—or at least a complication. As will be seen, in the $T_{1\rho}^H$ method we use, the extracted CR and NC line shapes are not ideal in the sense that contributions from different parts of the CR (or NC) region are not equally weighted. Our discussion later regarding the method will take into account this distorted polarization profile, especially in the context of the possibility that defects, so identified, might actually be concentrated at the CR/NC interface instead of being distributed throughout the crystalline region.

Very long acquisition times were needed in order to obtain spectra of the CR region (we shall call these "CR" spectra) that had a sufficiently good signal-to-noise ratio so that intensities of the order of 0.001 times the intensity of any parent resonance could be identified.

In cases where the defect concentrations were lowest, 10–12 days of scanning was required in which about 100 000 scans at each spin-locking time were averaged; 3–4 days of scanning was typical. Block averaging was used throughout in order to minimize the influence of long-term spectrometer drift. Typically, a 2 Hz exponential multiplication was applied to the signal prior to Fourier transformation; this choice represents a compromise between improving the signal-to-noise and maintaining the resolution necessary for identifying these very weak defect resonances.

For this kind of work one must be careful to avoid chemical contamination in handling. Moreover, one needs a probe which, under CPMAS conditions,[29] has no overlapping background signals originating from the probe or from the rotor, its caps, or spacers. This probe qualified in that regard.

Results

Sample Characterization. In Table 1 we list the iPP samples which were investigated, along with information about molecular mass, total defect concentration or fraction, f_D, melting point (T_m), estimates based on WAXS patterns of the fraction of crystalline material in the γ form (f_γ), and crystallinities as determined by DSC and, in this work, by NMR. These latter parameters pertain only to those samples cooled at 1 °C/min. Sample designations encode four items: catalyst ("M" for metallocene and "Z" for Ziegler–Natta), molecular mass in g/mol, total defect concentration in mole fraction, and, finally, an indication of the dominant type of defect ("S" for stereo defects, "R2" for regio 2,1 defects, and "R3" for regio 1,3 defects—each type of defect will be discussed more fully presently.) In Table 2 there is more detail regarding the defect populations (or concentrations), where the stereo-type defect concentrations are broken down further into pentad[1] fractions.

Method for Isolating the Spectrum of the Crystalline Regions. In Figure 1 we compare spectra taken with two spin-locking times, 0 and 8 ms, and illustrate how we take linear combinations to isolate the "CR" and the "NC" line shapes for sample M346-1.12S. In this figure, the top two overlaid spectra are the experimental spectra where the 8 ms SL spectrum is multiplied by 1.25 in order to produce a contribution from the CR region equal in magnitude to that of the 0 ms SL spectrum. Thereby, the diminished contribution from the broader NC carbons in the former spectrum is more clearly visible. The middle spectrum is that of the CR regions, and it is obtained from a linear combination of these two spectra where the dominant contribution is from the 8 ms SL spectrum. The amount of the 0 ms SL spectrum that is subtracted to obtain the CR spectrum is determined by the criterion that no regions of negative intensity are allowed in the spectral wings of each resonance where the NC carbons exclusively contribute. Finally, in Figure 1, the lower spectrum, i.e., the NC spectrum (vertically amplified ×3 with respect to the size of the NC contribution in the 0 ms SL spectrum), is another linear combination whose dominant contribution is the 0 ms SL spectrum where some 8 ms SL line shape is subtracted. This NC spectrum possesses broad features which are normally associated

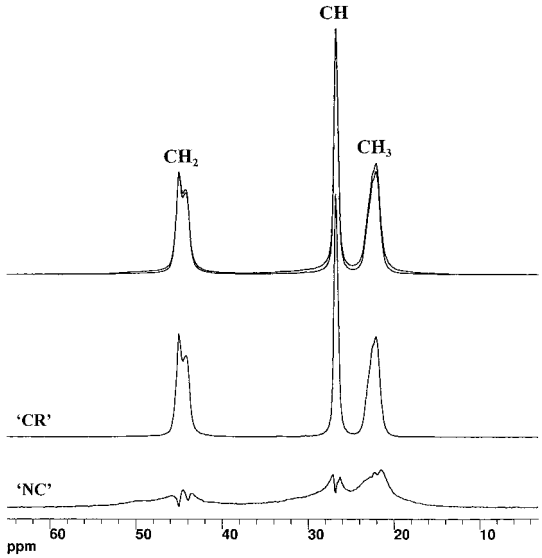

Figure 1. The 25 MHz CPMAS spectra of iPP sample M346-1.12S illustrating the method of separating the spectra of the crystalline (CR) and the noncrystalline (NC) regions. Top: overlay of experimental spectra with two spin-locking (SL) times (0 and 8 ms) that precede the 0.7 ms cross-polarization (CP) time. The 8 ms SL spectrum is multiplied by 1.25 so as to equalize the CR contributions. The weaker wings are associated with the 8 ms SL spectrum and indicate that the ratio of the CR to the NC contributions increases at longer SL time. This different ratio allows one to take linear combinations of these two spectra for generating the "CR" and the "NC" line shapes whose shapes are dominated by the 8 ms SL and the 0 ms SL spectra, respectively. For clarity, the NC spectrum is multiplied vertically by 3.

with less ordered chains; however, also apparent is what appears to be negative-going intensity in the regions of the sharper lines. One might guess that too much of the 8 ms SL line shape was subtracted; however, if one subtracts less of the latter line shape and eliminates evidence of the negative-going peaks, then the NC line shape takes on significant and modestly sharp contributions in the region of the CR resonances. So obviously there is some judgment and choice made in obtaining the NC line shape, and since this judgment may seem somewhat arbitrary, we will digress briefly to a more detailed discussion of what these line shapes represent. This will lead to a better understanding of the results.

In this discussion of the method, two perspectives are important. First, modeling the morphology simply as a two-phase system, i.e., CR and NC, is an oversimplification. Indeed there is an interface, and it is ludicrous to assume that chains should go from fully ordered (CR) to disordered (NC) without a finite region where this transition is made. Therefore, if either the CR or the NC line shapes possess some nonideal features (e.g., the negative-going intensities in the NC spectrum), the origin of these nonidealities may well be that there are more than two domains (or component line shapes) contributing to the spectrum. Second, the method we are using, where differential $T_{1\rho}{}^{H}$ relaxation is responsible for altering the ratio of CR and NC contributions to the line shape for different SL times, is itself nonideal, given that spin diffusion[30] proceeds during spin locking. Spin diffusion is the movement of polarization, via a network of abundant, dipolar-coupled like spins (e.g., protons) in the presence of a polarization gradient. The presence of spin diffusion is essential for giving us confidence that the ^{13}C signal strength per carbon at the defect is the same as that for the surrounding,

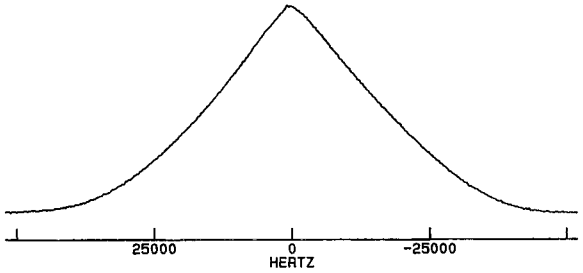

Figure 2. The 200 MHz proton spectrum associated with the Bloch decay of the M200-0.42R2 sample. Note that there is no evident "narrow" component which one might easily associate with the NC chains.

nondefect carbons. On the other hand, spin diffusion introduces nonideality into the separation of CR and NC signals since, even if there were infinitely sharp boundaries separating the CR and the NC regions, the profile of the polarization after, say, 8 ms of SL, will *not* be a step function in the vicinity of the CR/NC interface. After 8 ms of spin locking, for example, the NC protons near the interface will have a higher polarization, relative to the average NC proton polarization; this situation results from spin diffusion and from the longer $T_{1\rho}{}^{H}$ (and more sustained polarization) of the CR region.

In the discussion of the method that follows, we will treat the influence of spin diffusion in an ideal, lamellar two-phase system with sharp boundaries, fixed long period and well-defined, distinct $T_{1\rho}{}^{H}$'s throughout each region. We will see how the CR and the NC line shapes are nonuniformly weighted across each region. After seeing the inherent biases in the method, we will be in a better position to interpret the CR and the NC line shapes in terms of the true heterogeneity of the morphology, including the interface.

For our idealized semicrystalline morphology we will choose a long period which is close to that found experimentally in these iPP samples, and we will use NMR parameters that agree with the experimental observables. Thus, we adopt a lamellar morphology with a long period of 16 nm and a crystalline fraction of 0.60 so that, ignoring density differences, the CR thickness will be 9.6 nm and the NC thickness will be 6.4 nm. We assign spin diffusion constants $D(\mathrm{CR}) = 0.35\ \mathrm{nm}^2/\mathrm{ms}$ and $D(\mathrm{NC}) = 0.175\ \mathrm{nm}^2/\mathrm{ms}$; the former is a good estimate[31,32] which also incorporates the fact that during spin locking the spin diffusion constant (along with the proton−proton dipolar interaction) in the rotating frame is halved relative to the spin diffusion constant in the laboratory frame. The magnitude of D(NC) is more of a guess where it is assumed that the mobility of the chains in the NC will reduce the line width by about a factor of 2 relative to the line width associated with the CR regions. Figure 2 shows the proton spectrum of the M200-0.42R2 sample. While the CR and NC contributions are not separated in this spectrum, it is clear that, unlike polyethylene, there is no distinct narrow component sitting on top of the broader crystalline component. Hence, motion in the NC region is of limited amplitude, and the value assigned to D(NC) may, if anything, be a bit low. The remaining parameters, i.e., the 0.7 ms cross-polarization time (involving spin locking on the protons), a pair of preceding spin locking times of 0 and 7 ms, and $T_{1\rho}{}^{H}(\mathrm{NC}) = 4.17$ ms and $T_{1\rho}{}^{H}(\mathrm{CR}) = 83$ ms, are all chosen to mimic the experimental parameters or, in the case of the $T_{1\rho}{}^{H}$'s, the calculated intrinsic $T_{1\rho}{}^{H}$'s one would need in order to see the

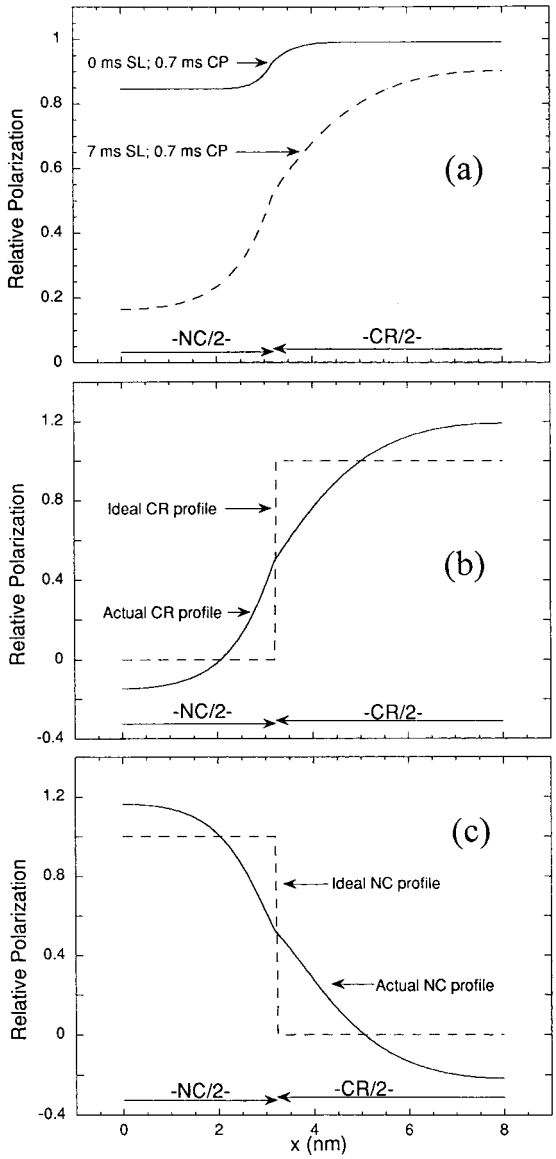

Figure 3. Computational modeling (top panel) of the proton polarization as a function of distance and SL time assuming an idealized two-phase lamellar morphology with a long spacing of 16 nm and other parameters chosen to reproduce the data observed for sample M346-1.0S (see text). Influences of both spin diffusion and differential $T_{1\rho}^{H}$'s are accounted for. The plots cover only half the long spacing (= 8 nm) with the NC region on the left, the CR region on the right, and the idealized interface at $x = 3.2$ nm. The ordinate is the average proton polarization per spin after 0 and 7 ms of SL followed, in both cases, by 0.7 ms of CP. Via CP, these same profiles pertain to the ^{13}C polarization per spin in the ^{13}C experimental spectra. The lower panels illustrate the nonideality of the deduced "CR" and "NC" spectra in terms of the nonuniform weighting of polarization arising from different morphological regions. The middle panel contrasts the idealized ^{13}C polarization with the ^{13}C polarization profile that is, in turn, associated with the deduced CR spectrum. The lower panel is the same comparison pertaining to the spectrum of the NC regions. Note that for both the deduced "CR" and the deduced "NC" spectrum, contributions from the middle of the desired region are exaggerated. These contributions diminish as one approaches the interface; in addition, contributions from the nondesired region are significant at the interface, and then they diminish, even going negative as one moves to the center of that region.

observed change in both amplitude and in CR/NC intensity ratio.

Figure 3 consists of three panels, each displaying along the abscissa a distance of 8 nm (half of the 16 nm long period), extending from the midpoint of the NC region to the midpoint of the CR region. The sharp, idealized interface is at 3.2 nm. The top panel shows the profile of the polarization as a function of distance, corresponding to each of the experimental spectra taken at 0 and 7 ms of spin locking. Polarization, as we use the term here, is a reduced quantity which represents the *ratio* of the experimental, average polarization per spin to the Boltzmann-equilibrium average polarization per spin. We have assumed that the ^{13}C polarization is directly proportional to the local proton polarization *at the end of the cross-polarization period*. Note that the polarization boundary is quite sharp in the SL = 0 profile for two reasons: (a) the spin-locking time during cross-polarization is relatively short (0.7 ms) so diffusion is limited by time, and (b) polarization gradients at the boundary are just beginning to build up (polarizations are equal at the beginning of spin locking) so that the average driving force for polarization transport is still quite low. In contrast, after 7 ms of SL plus 0.7 ms of CP, both the longer time and the larger overall gradients make the polarization profile more gradually changing in the vicinity of the interface. If, therefore, we now take linear combinations of spectra with these two profiles of polarization, we can gain some insight into the actual polarization weighting for the resulting line shapes when we claim to have either a CR or a NC spectrum. This is illustrated in the middle panel for the CR line shape and in the lower panel for the NC line shape. There, the dotted lines represent the ideal case and the solid line the actual weighting of polarizations. The sum of the CR and NC amplitudes at each abscissa value is identically 1; hence, these two curves are really mirror images reflected about the line corresponding to a polarization of 0.5.

It is clear from Figure 3 that for, say, the "CR" line shape the deviations from the idealized polarization profile are substantial. Contributions are greater than ideal from the interior of the CR domain, and they are less than ideal from the CR side of the interface. In addition, there is a positive contribution from the NC side of the interface and an offsetting negative contribution from the interior of the NC region. At the same time, the *integrated* polarizations across the CR and NC regions give respective average values of 1.00 and 0.00, just like the ideal profile. (In each of the CR and NC regions of Figure 3b, positive and negative deviations from the ideal profile offset one another; integral magnitudes are respectively 8.4% and 4.9% of the total CR integral.) From Figure 3 we can say that if we apply the $T_{1\rho}^{H}$ method, even if there were an ideally sharp interface, we will not be able to isolate an ideal polarization profile for the CR contribution; i.e., there will always be a stronger contribution from the interior of the CR region and offsetting negative and positive contributions from the NC interior and the NC side of the interface, respectively.

We should extract two more perspectives based on Figure 3 in recognition of the nonideality of the "CR" and the "NC" line shapes. First, only if the line shape is *not* a function of position in a given phase will the separation into CR and NC line shapes work out well, i.e., be free of apparent artifacts. Thus, on the basis of Figure 3c, we can go back to the "NC" line shape of Figure 1 and appreciate the origin of the "negative-going", narrow-line contributions. The latter indicate that the resolution in the interior of the CR regions is

better than that near the interface. This should come as no surprise since the packing should be better (and the lines narrower) in the interior of the crystalline regions. This is a common observation in our experience with semicrystalline polymers; i.e., this characteristic is not just associated with the presence of defect structures. Thus, when we use the term "CR region", we indicate a single region while admitting that the spectral signature of that region does *not* support the view that this is a uniformly well-organized region.

The second perspective is that the separation into CR and NC contributions does the worst job close to the interface. Thus, if one were to argue that defects, which would go into the crystal lattice at some energetic cost, should concentrate at the interface, then one should also look carefully at the spectral observations to see whether these defects were either distributed throughout the CR regions or concentrated at the interface. We will look for evidence of high concentrations at the interface. To set the stage for the arguments we invoke later, we note two things now: (a) On the basis of the profiles of Figure 2, if there is a very high concentration of defects at the interface, the spectral signature of those defects, while relatively strong in the CR spectrum, should be weaker, but still visible, in the NC spectrum. (b) In iPP, we are unable to identify resonances associated with defects in disordered (NC) regions. Hence, all experimental evidence concerning the presence of defects at the interface relates to those defects that exist in a context of significant order, i.e., the CR side of the interface.

While we elect not to do other calculations such as those of Figure 3, for the case of finite interfaces, we note that if parameters such as $T_{1\rho}^{H}$ and the spin diffusion constant are monotonically changing functions across the interface, then the qualitative features of the CR and NC polarization profiles seen in Figure 3 will also typify the polarization profiles that pertain to the morphology with finite interfaces. The only difference is that the polarization profile at time t_{sd} in the presence of interfaces will closely resemble the profile at time ($t_{sd} + \Delta t_{sd}$) in the absence of interfaces,[31] where Δt_{sd} would most likely be of the order of 1 ms. Thus, there is considerable generality in the polarization distortions represented in Figure 3 for the CR and the NC spectra; the presence or absence of a finite interface only changes the amplitude of the distortions to a small degree.

^{13}C Spectra Associated with Stereo and Regio Defects. In Figure 4, 25.2 MHz CR spectra of six of the seven samples are shown. The top three spectra (Z250-0.9S, M346-1.0S, and M335-2.34S) are samples with increasing defect concentration and a dominance of stereo defects. Third and second from the bottom are spectra of M327-0.42R2 and M236-1.17R2 whose main defect type is the 2,1 erythro regio defect. The bottom spectrum is that of M9.8K2.4, the low molecular weight sample with a dominance of 1,3 defects. All of these samples were melt crystallized at a cooling rate of 1 °C/min. As can be seen in Table 1, there is a significant range of melting points represented in these samples, and one expects a range of crystal perfection in these samples. Also, the greater is the concentration of defects, the higher the γ-content of the crystalline phase.[21] While the methine resonance, centered at 27.0 ppm, is quite narrow and very similar from sample to sample, the methyl resonance (21−24 ppm) and the methylene resonance (43−46 ppm) are much broader and show some fine structure. In particular, the methyl resonance

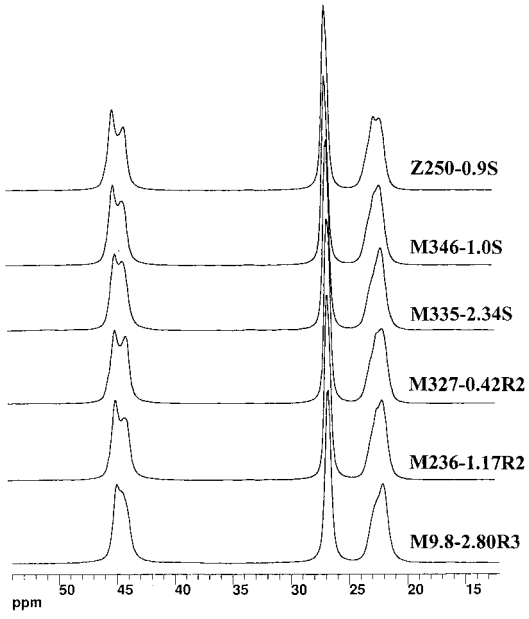

Figure 4. CR spectra of several indicated melt-crystallized (1 °C/min) iPP samples used in this study. Note the variation in shape for both the CH_3 and the CH_2 resonances.

appears to be made up of three strongly overlapping resonances centered about 22.0, 22.7, and 23.1 ppm, the latter resonance appearing as a shoulder. The methylene resonance, on the other hand, usually appears as a doublet whose components resonate near 44.1 and 45.1 ppm; albeit, the samples richer in the γ-phase tend to show a slightly smaller splitting. Since all of the proposed crystal forms of iPP[15−20] share the feature that the conformation of each chain is a 3_1 helix, the qualitative interpretation of the variation in line width seen in Figure 4 is that the methine resonance is narrow because the methine carbon is most shielded in the interior of the helix while the methyl and methylene resonances are closer to the outside, experiencing stronger intermolecular perturbations from crystal packing effects. The inequality of amplitudes for the multiplet features, even for those samples (e.g., M327-0.42R2) of nearly pure α-phase, is understood[33] from the point of view that the unit cell does not have a symmetry commensurate with the 3_1 helical symmetry. Hence, the intermolecular interactions experienced by consecutive methylene or methyl carbons along a helix can be dissimilar.

It has been demonstrated quite convincingly[34] that a very well-annealed α-phase spectrum gives a methyl line shape for the CR region which consists of a downfield peak about twice the intensity of the upfield peak. This same cited study also reported the ^{13}C CPMAS spectrum for the γ-phase, and it was claimed that the spectrum of the γ-phase showed the reverse trend, namely, that the upfield methyl peak was about twice that of the downfield peak, even though the positions for the methyl resonances were similar for the α- and γ-phases. Unfortunately, the rf amplitude used in this cited study was inadequate for defining the methylene multiplet relationships with respect to the α- and γ-phases. In a somewhat contrasting interpretation of the line shape, Caldas et al.[35] did a very careful annealing study of spun iPP fibers and saw the methyl line shape change quickly, especially in the 150−160 °C range. One of the main points about their interpreta-

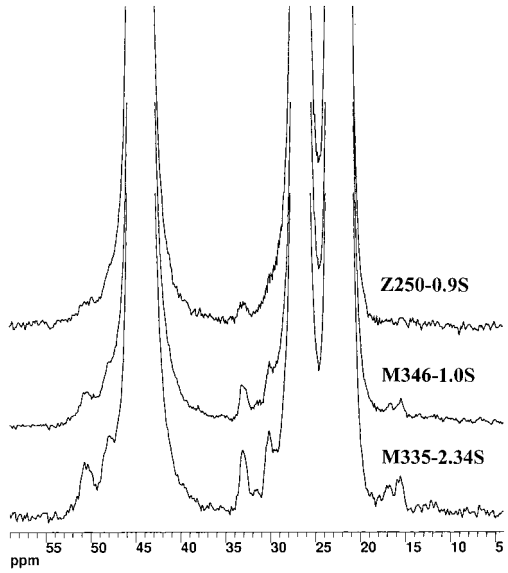

Figure 5. Vertically expanded (×64 relative to Figure 4) CR spectra of the samples whose dominant defects are stereo defects: Z250-0.9S (top), M346-1.0S (middle), and M335-2.34S (bottom). The two lower spectra are metallocene iPP's, and the upper spectrum is that of a heterogeneous Ziegler−Natta pseudofraction. The weak resonances near 16, 30, 33, 47 and 50 ppm are associated with the stereo defect because the intensities are proportional to the overall stereo-defect populations in the metallocene iPP's; at the same time, the defect-resonance intensity is relatively weaker in the Ziegler−Natta product for reasons discussed in the text.

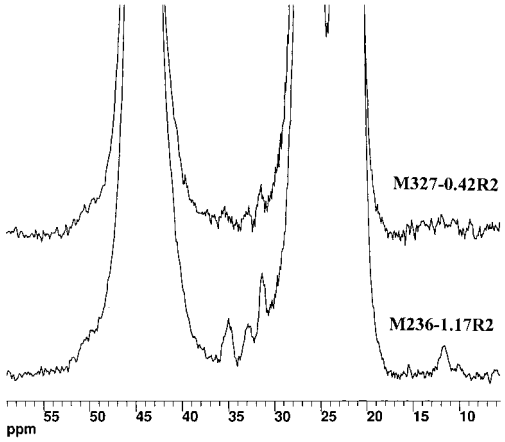

Figure 6. Vertically expanded (×128 relative to Figure 4) CR spectra of the samples whose dominant defects are regio 2,1 erythro defects, one of two types of head−head defects; M327-0.42R2 (top) and M236-1.17R2 (bottom). Resonances around 12, 31, 33, and 35 ppm are ascribed to this defect. Signal-to-noise is worse than in Figure 5 since the overall concentration of these defects is smaller; moreover, a smaller fraction of these defects find their way into the CR region. Defect resonances in the top spectrum are the order of 0.1% of each main backbone resonance.

tion of the changes in the methyl line shape involved noting that a growth of the central component of the methyl multiplet (as well as a decrease in the intensity of the downfield shoulder) is associated with some transformation to the α_2-phase, a phase[16,17] which is claimed to have a $P2_1/c$ space group and order with respect to chain directionality. (In the spectra of Figure 4 the Z250-0.9S and the M327-0.42R2 samples have the higher α_2 contents by that interpretation.) In contrast, the α_1-phase, more typical of faster crystallization at lower temperatures, has a $C2/c$ space group, and there is randomness with respect to chain directionality.[15] An ambiguity regarding the interpretation of Caldas et al. is that no information was given about the level of defects in the iPP, and there could, depending on the level of defects, also be concurrent α/γ transformations[21] during annealing that would have an impact on the line shape changes they observe.

Owing to ambiguities about the interpretation of the NMR line shapes, we rely on X-ray analysis to indicate the level of γ-phase[21] using published[18,36] X-ray assignments for the γ- and α-phases. As to distinguishing the α_1-phase from the α_2-phase, we have not attempted to make those distinctions either. In defense of the α_1/α_2 distinction being real, it is clear that there is not just a single level of perfection associated with the packing of the α-phase. For a sample which only forms the α-phase, the methylene and methyl line shapes are dependent on crystallization history in a way which is **not** limited to changes in line width[35,37] (see ahead to Figure 12 also). The observed changes in overall shape, although not extensive, are consistent with small alterations in the packing of the unit cell.

Figures 5 and 6 show vertically expanded (×64 and ×128, respectively) CR spectra of five of the six samples in Figure 4. In Figure 5, the spectra of those samples having dominant stereo defects are shown while the spectra in Figure 6 correspond to samples where the erythro 2,1 defect is dominant. In Figure 5, the lower spectrum represents a sample where the concentration of defects is about twice that of the sample represented in the middle spectrum (see Table 2); both samples are metallocene products. For comparison, the top spectrum is that of the Ziegler−Natta pseudofraction. The top and middle spectra represent samples with similar stereo-defect concentrations. The lower spectrum represents the highest concentration of stereo defects although about 25% of the defects are not stereo (see Table 2). Despite this "contamination" with other defects, we expect that the most intense defect resonances observed would arise from the stereo defects. In the lower spectrum, there are six weak, but relatively well defined, resonances at about 15.6, 16.8, 30.1, 33.1, 47.9, and 50.6 ppm. In the middle spectrum, these resonances appear in the same positions with correspondingly weaker intensities, consistent with the lower concentration of stereo defects. The sample whose spectrum is inconsistent, intensity wise, with this scheme is the Ziegler−Natta pseudofraction. There, the most unambiguous defect resonance is at 33.0 ppm; the next most obvious resonance of the foregoing set is the shoulder near 50 ppm. The shoulders near 30 and 48 ppm are just barely discernible, and one would be hard pressed to call these resonances in the absence of the other spectra. The expected resonances near 16 ppm are really not identifiable above the noise level. In any case, the identifiable weak defect resonances in the Ziegler−Natta material are at least consistent with the stereo-defect resonances of the metallocene iPP's.

We are interested in the explanation for the considerably smaller CR concentration of stereo defects in the Ziegler−Natta pseudofraction compared with that in sample M346-1.0S since the overall concentration of defects, and in particular, the stereo defects, are very similar (Table 2). Aside from the differences in polymerization catalysis, a phenomenological difference is that the Ziegler−Natta pseudofraction is pure α-phase, while

the metallocene iPP has a significant fraction of γ-phase (see Table 2). The fact that the γ-phase is absent in the Ziegler−Natta pseudofraction, despite comparable defect concentrations, means that there is something different about the defect population in these two materials. The added recognition in Figure 5 that the Ziegler−Natta pseudofraction has a lower concentration of stereo defects in the CR lattice strongly supports the conclusion that fewer of the stereo defects were available for crystallization, relative to how many were available in the M346-1.0S sample. Supposing that fewer defects were available for those chains which crystallize, one would also expect a higher fraction of the α-phase, as is observed, since, all other things being equal, a higher fraction of defects promotes an increase in the fraction of the γ-phase.[21] In principle, we must also consider the possibility that the α-phase rejects the stereo defect to a larger degree than the γ-phase; nevertheless, for the argument presented here, we ignore this possibility since it cannot explain why one of these samples has considerable γ content and the other does not. Thus, we conclude that our findings provide further support that iPP's, synthesized using heterogeneous Ziegler−Natta catalysts, produce chains with varied populations of stereo defects.[38−40] Since, as we will see, there is some discrimination against incorporating the stereo defect into the CR region, chains with a higher defect concentration will have a higher probability of not crystallizing; hence, in the Ziegler−Natta pseudofraction, the chains available for crystallization will have an average concentration of defects which is lower than the overall concentration of defects. In contrast, if the metallocene product is uniform in this sense, owing to the homogeneous nature of the polymerization, then the concentration of defects in the crystallizing chains will be about the same as the overall concentration.

Aside from the chemical shifts of the defect resonances, one would like to know their relative intensities and assignments. Regarding intensities, the partial overlap of the defect resonances with the main backbone resonances makes integration of defect resonances more difficult, especially since we cannot assume Gaussian or Lorentzian line shapes because the backbone resonances do not possess well-behaved line shapes. In principle, the relative integrals should lend some clue about the assignments, especially if the integrals are in the ratio of small whole numbers. We will defer a discussion about the method of extracting integrals. For now, we simply note that the peak height is highest and the line width narrowest for the defect resonances at 30 and 33 ppm. By analogy to the relative line widths of the backbone resonances, we are thus strongly inclined to assign these resonances to methine carbons at or near the defect sites. Likewise, on the basis of both chemical shift and line width, the 47 and 50 ppm lines are most likely to be methylene carbons. Finally, the doublet near 16 ppm most likely represents methyl carbons. The argument just invoked is the postulate that for a CR defect, held in a well-defined lattice of its neighboring chains, the spread of conformations should be modest at best; thus, one expects the defect resonances to have line widths that are similar to those of the backbone carbons in the CR lattice. To summarize the deductions from Figure 5, there are six defect resonances associated with the stereo defect, probably two resonances from each chemically distinct kind of carbon. The unresolved issues relate to the relative and absolute integrals of these resonances and the true number of distinct carbon resonances associated with each defect.

We treat the spectra in Figure 6 in a way similar to those of Figure 5 in the sense that we look for a pattern of resonances associated with the erythro 2,1 defect, where the intensities follow the known overall concentration of defects. The suite of identifiable resonances, seen more clearly in the M236-1.17R2 spectrum and recognizably present in the M327-0.42R2 spectrum, includes lines at about 12 (with a possible shoulder near 10 ppm), 31.6, 33.1, and 35.3 ppm. The M236-1.17R2 sample has some contamination (about 21% of the total defects) from the stereo defect so some adjustment (discussed in connection with Figure 9) to the defect resonance pattern must be made in order to isolate the influence of the 2,1 defects. A comparison of these chemical shifts with those defect resonance positions assigned earlier to the stereo defect indicates that both the 12 and the 35.3 ppm resonances are well separated from the stereo defect resonances; hence, the integrals of these resonances, relative to the integrals of the backbone resonances, should yield the concentration of 2,1 defects in the CR regions, provided again that we know how many distinct resonances arise from each 2,1 defect. If we again look at line width differences and chemical shifts as an indication of the kind of carbon giving rise to the defect resonances, we would assign the 12 ppm carbon to a methyl carbon, the 31.6 ppm line to a methine, and the 35.3 ppm line to a methylene. The 33.1 ppm line is not so clear. A caveat for these latter two guesses at assignments is that the 2,1 defect entails a change in the head-to-tail sequence and thereby calls into question the level of exposure to neighboring molecules for the methine and methylene carbons at the defect. Within the signal-to-noise limitations, the 2,1-defect intensities in these two spectra are proportional to the corresponding, known overall concentrations of the 2,1 erythro defects. Also, while we do not show the CR spectrum of the M200-0.42R2 sample, its CR spectrum is indistinguishable from that of the M327-0.42R2 sample. We choose to display the latter spectrum because we did more extensive signal averaging on it.

From Figures 5 and 6, it seems evident that some defects, both stereo and 2,1 regio, are found in the crystal. Actually, we also considered two alternate possible explanations for these observed weak resonances; these alternatives did not require the defects to be distributed throughout the CR regions. First, the narrow resonances might simply arise from tight loops at or near the lamellar surface. Second, the resonances could be associated with the defects; however, those defects might be highly concentrated at the interface and not be found in the interior of the CR regions. The first possibility is pretty easy to dismiss on the basis of two observations: (a) the very different pattern of resonances seen for the stereo and the 2,1 regio defects and (b) the variation of these resonance intensities with defect concentration. (In the low defect concentration regime, the variation in the number of carbons in tight folds ought to vary more slowly than the defect concentration.)

The possibility that defects are highly concentrated at the interface requires a more complex response which, in the end, is a limited response because we do not claim equal insight into defect concentrations on

both sides of the interface. Also, it is a qualitative, not quantitative, response.

In the following arguments, we assume that if defects concentrate at the interface, they would probably be found on both the disordered and the ordered side of the interface. For defects on the disordered side of the interface, resonances should be quite broad, reflecting variations in conformation and in intermolecular potentials. Resonances from NC defects close to the interface are, on the basis of Figure 3, expected to contribute modestly to the CR spectrum; however, these resonances should be undetectable owing to the low overall concentration of defects and our inability to identify very weak, broad resonances that at least partially overlap with the resonances of the CR backbone carbons. Thus, there are two important implications of the foregoing statements, namely, (1) if there is a high concentration of defects on the disordered side of the interface we will not know this and (2) the observed, relatively narrow defect-resonance widths, similar to the line widths for the CR backbone carbons, strongly suggest a very ordered intermolecular potential surrounding those defects whose resonances are observed; i.e., if these defects are close to the interface, they must be on the CR side of the interface.

If we suppose, for the sake of argument, that the CR defects whose resonances we observe are highly concentrated, say, within a 1 nm layer on the CR side of the interface, then, on the basis of the profiles of Figure 3, one would expect that these defect resonances should be visible in both the CR and the NC spectrum. In fact, when the CR and NC polarization profiles in Figure 3 are normalized such that their intensities add up to the spectrum with 0 ms spin-locking time, the predicted defect-intensity ratio is 1.8:1 in the CR and NC spectra, respectively. This 1.8:1 ratio is predicated on there being a uniform distribution of defects within this 1 nm layer. If there is a gradient of increasing concentration toward the interface, then this ratio gets even smaller, and the intensity in the NC spectrum gets larger. Figure 7 shows spectra that test this prediction for sample M335-2.34S, the sample with the highest stereo-defect concentration. Figure 7 shows vertically amplified 0 ms SL, CR, and NC spectra, properly normalized so that the latter two spectra add up to the 0 ms SL spectrum. The result is that, contrary to the hypothesis that all defects lie within 1 nm of the interface, there is no evidence in the NC spectrum of any maxima or shoulders at the positions of the defect resonances. Of course, because of strong overlap with the backbone resonances in the NC spectrum, it is harder to say that the resonance contributions from the defects are truly negligible. Yet, the fact that those defect resonances identified in the CR spectrum are also easily seen atop the rolling NC backbone resonances in the 0 ms SL spectrum suggests that the defect intensity ratio in the CR spectrum versus the NC spectrum is at least 5:1 and definitely not near 1.8:1. To get a ratio like 5:1 in Figure 3 would require a layer of 2 nm thickness and uniform defect concentration in the layer. If defects are concentrated at the interface, the postulate of uniform concentration is not reasonable; hence, to explain the experimental findings, we conclude (in qualitative fashion) that at least some defects are found in the interior of the CR domains, and while there may be some concentration gradient toward the interface, the defects are not highly concentrated on the CR side of the interface.

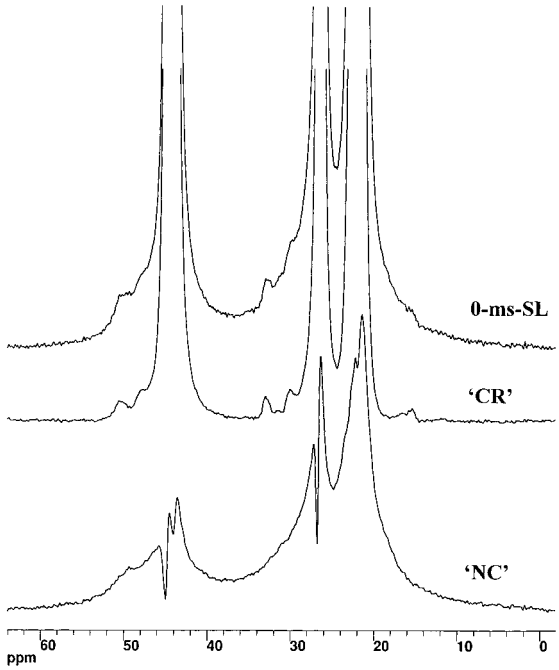

Figure 7. Spectra of the M335-2.34S sample from which spectra it is deduced that defects are not highly concentrated on the CR side of the interface (see text): top, 0 ms SL spectrum; middle, CR spectrum; bottom, NC spectrum plotted so that the summed intensity of the two lower spectra equals that of the upper spectrum. The critical observation is that one cannot identify any stereo-defect intensity (e.g., near 33 ppm) in the NC spectrum, even though, according to Figure 3, the NC polarization profile should have a nonnegligible positive contribution from defects close to and on the CR side the interface.

A final argument in favor of the defects, at least in sample M335-2.34S, being found in the interior of the CR domains is that the T_1^C's of those defect resonances that are downfield of the methine backbone resonance are comparable to the T_1^C's of the backbone methine and methylene carbons. Owing to signal-to-noise issues, the foregoing statement is based, not on a full set of T_1^C data, but on comparable reductions in the amplitudes of the backbone and defect resonances after a 5 s period of T_1^C decay in a Torchia-type T_1^C experiment.[41] If the defects were concentrated at the interface, the average T_1^C of the defects would be expected to be considerably shorter than the T_1^C's of the backbone methine and methylene carbons.

We now return to the matter of determining the average concentration of stereo defects in the CR regions. To determine this quantity, we must be able to (a) integrate the defect resonances relative to the backbone resonances and (b) determine how many distinguishable defect resonances are associated with each defect. The best signal-to-noise ratio for the stereo-defect resonances is found in the M335-2.34S sample, which has the highest stereo-defect content. So we seek to analyze the CR line shape of this material. If we look at Table 2, we also notice that the M335-2.34S sample contains other defects, namely, 0.23% erythro 2,1 defects, 0.30% threo 2,1 defects, and 0.14% 1,3 defects. In Figure 8 we illustrate how we make a zeroth-order correction for the erythro 2,1 defects. The middle spectrum is the CR line shape of sample M335-2.34S. The upper spectrum is that of the M327-0.42R2 sample. The total intensities of these two spectra are inversely proportional to their respective erythro 2,1 defect concentra-

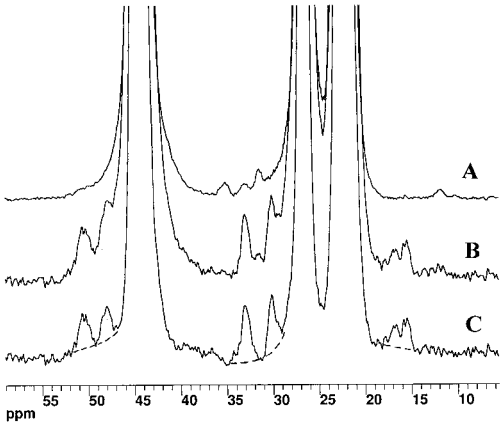

Figure 8. Illustration of a zeroth-order correction to the CR defect intensities of the M335-2.34S CR spectrum (middle). Spectral contributions of the 2,1 erythro defect, as embodied in the properly scaled CR spectrum (top) of the M327-0.42R2 sample are subtracted, and in so doing, a more resolved spectrum of those stereo defects appears in the difference spectrum (bottom). Corrections for the regio 2,1 threo defect are not made because we do not know what the spectral signature of this defect is; however, this correction should be of comparable magnitude to the corrections represented by the top spectrum. Dashed lines indicate the baseline assumed for integrating the defect resonances in the difference spectrum.

tions. The lower spectrum is the difference spectrum where the defect resonances belonging to the stereo defect should have the same intensities as in the middle spectrum. Since about half of the backbone intensity has been subtracted in the difference spectrum, the stereo-defect resonances are now more clearly visible in that they have less overlap with the backbone resonances. Obviously, we have not made a correction in this procedure for the threo 2,1 defect or for the 1,3 regio defect. As we will presently see, the 1,3 defect does not give rise to any distinct defect resonance in the CR spectrum. At the same time, the threo 2,1 defect may produce some pattern of CR resonances. However, this pattern of threo resonances is likely to be different from the pattern of the erythro defects; hence, we did not want to use the erythro pattern for the threo correction. Since the threo concentration is similar to the erythro concentration in M335-2.34S, any threo-defect corrections to the line shape for the stereo defects in the lower spectrum of Figure 8 will be comparably small to the corrections represented by the upper spectrum of Figure 8. This lower spectrum is the best spectrum we have for evaluating integrals of the defect resonances in the middle spectrum. From these integrals, along with the total integral of the middle spectrum, we can get $C(\text{stereo})_{CR}$, provided we know how many resonances each stereo-defect produces.

To obtain the integrals of the stereo-defect resonances in the lower spectrum of Figure 8, we integrated these peaks using three methods. Recall that we did not feel justified in assigning any regular shape to these resonances since the backbone resonances had non-Gaussian and non-Lorentzian shapes. The three methods were: (a) cut and weigh using the baselines indicated by the dotted lines in the lower spectrum of Figure 8, (b) electronic integration involving an estimation of the slope of the wings of the backbone resonances, and (c) use of scaled, shifted, backbone resonances in a spectral difference mode in order to null the intensity at the defect sites. All three of the above methods gave consistent results. The most reliable integrals came from the most isolated, least-overlapping resonances, i.e., those at 15−18 ppm, at 33 ppm, and at 51.5 ppm. It is very significant that, within ±10%, the integrals for all defect resonances are the same intensity, where the doublet in the 15−18 ppm range has a total intensity equal to the intensity of each of the other four stereo-defect resonances. This equality of defect intensities is the most compelling experimental argument for postulating that each stereo defect produces the entire suite of five observed defect resonances, the methyl defect showing multiplet character as did the backbone methyl resonance. Assuming that the ratio of the integral of any defect resonance to the integral of any backbone-carbon resonance gives $C(\text{stereo})_{CR}$, then $C(\text{stereo})_{CR} = 0.69 \pm 0.07$ for the M335-2.34S sample. This translates into a partitioning coefficient, $P_{CR}(\text{stereo}) = 0.36 \pm 0.05$, if we take half the mmmr pentad concentration to be the measure of the stereo-defect concentration. At the other extreme, $P_{CR}(\text{stereo}) = 0.48 \pm 0.06$ if we take the mrrm pentad concentration as a measure of the dominant stereo defect, i.e., the ...mmmrrmmm... defect which involves a single methyl being out of stereo sequence in an otherwise perfect iPP sequence. It is certainly true that the mrrm pentad defines a simpler and much more specific stereo defect than does the mmmr (= rmmm) pentad. The latter pentads will always be found bracketing a stereo defect, no matter how complex and clustered that stereo defect is, while the mrrm pentad is associated with a single, centrally located stereo error in a sequence of five monomers. According to Randall,[8] the most stereo-regular chains in a Ziegler−Natta iPP have stereo defects that are dominated by the mmrrmm heptad. That seems to be the case for these metallocene products as well, judging by the fact that in Table 2, for the M335-2.34S and M346-1.0S samples, the ratio 2[mrrm]/[mmmr] is about 0.74, suggesting that about $^3/_4$ of the stereo defects involve just a single methyl group out of stereo sequence. The remaining 26% of the stereo defects involve clusters of stereo errors that span more than one monomer. While we do not know the details of the structure of these other, more complex stereo defects, we can point out two considerations that help us choose which of the above $P_{CR}(\text{stereo})$ values is more reasonable. First, it is likely that those sequences, which involve defect structures extending over multiple monomer units, will be more strongly rejected, compared to the simpler mrrm defect, in the crystallization process. Second, for any of these more complex stereo defects that find their way into the CR region, the chemical shift patterns are likely to differ from the pattern of the mrrm pentad. Therefore, on the basis of the foregoing reasoning, we suggest that a more reliable estimate of $P_{CR}(\text{stereo})$ is 0.48 ± 0.06 where the fate of the non-mrrm stereo defects is left as a complete unknown.

In terms of determining $C(\text{stereo})_{CR}$, recall that it is critical to establish how many distinct defect resonances are associated with each defect. For each mrrm defect, we assumed that one carbon at each of five distinct chemical shifts was involved. This was based on approximately equal integrals. We also have been working hard at trying to calculate chemical shift patterns for carbons near a mrrm defect. We have employed the following process: (a) Build an α-type CR lattice and place both a perfect chain and a "defect chain" (with the defect centrally located with respect to chain ends) in a central-stem position in this lattice. Then, energy

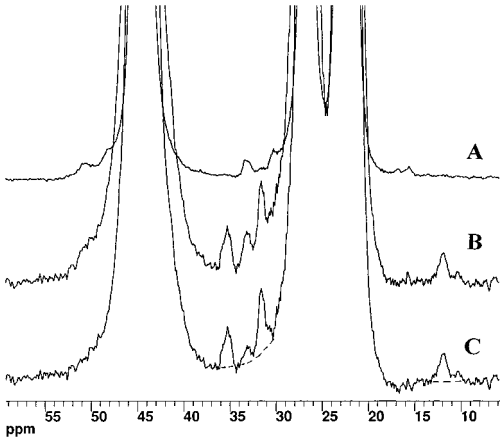

Figure 9. Illustration of a zeroth-order correction to the CR defect intensities of the M236-1.17R2 CR spectrum (middle). Spectral contributions of the mrrm stereo defect, as embodied in the properly scaled CR spectrum (top) of the M346-1.0S sample are subtracted, and in so doing, a slightly more resolved spectrum of those regio 2,1 erythro defects appears in the difference spectrum (bottom). Owing to a small population of 2,1 erythro defects in the M346-1.0S sample, the 2,1 erythro defect intensity in the difference spectrum is 4% lower than in the middle spectrum. Note the substantial weakening of the resonance at 33 ppm as a result of the subtraction. Dashed lines indicate the baseline assumed for integrating the defect resonances in the difference spectrum.

minimize each chain in the fixed lattice of the neighboring chains. (b) Take a sequence of about 7.5 monomers from the central region of these two energy-minimized conformations, replace terminal methylenes with methyls, and perform chemical shift calculations for these isolated oligomers. (c) Compare shifts of corresponding carbons for the perfect and the defective chains and look for agreement with experimental shift differences. We are optimistic about the success of this effort. In a separate paper[42] we will detail our calculations and show strong support for the notion that each stereo defect produces five distinct defect resonances.

We move now to a consideration of the erythro 2,1 defect as represented in the samples M327-0.42R2 and M236-1.17R2. This story is not as clear as it is for the stereo defect, in large part because of signal-to-noise limitations in that 0.95% was the highest concentration of 2,1 defects we could get for samples whose dominant defect was the 2,1 erythro defect. From Figure 6, as noted earlier, there seems to be a qualitative consistency in the position of the distinct defect resonances and in the approximate variation of defect-resonance intensity with overall 2,1 defect concentration. Figure 9 illustrates our attempt to isolate the spectrum of the 2,1 erythro defect. As in Figure 8, we attempt to subtract, from the spectrum with the highest defect concentration, an appropriate fraction of intensity from another spectrum that represents the "contaminating" stereo-defect concentration. Thus, in Figure 9, from the spectrum of M236-1.17R2 (middle), we subtract a portion of the M346-1.0S spectrum (top), normalized so that the stereo-defect intensities are equalized, to create the difference spectrum (bottom). Again the defect resonances in the difference spectrum should be the best representation of the pure 2,1 erythro-defect resonances. These 2,1 defect resonances should have an intensity 96% of the corresponding 2,1 defect intensities in the middle spectrum, because the M346-1.0S sample has a small amount of 2,1 erythro defects. As can be seen from the top spectrum, the only resonance that will be strongly affected by the stereo-defect correction is the resonance at about 33 ppm. That latter resonance changes from a significant resonance in the middle spectrum to a minor resonance in the difference spectrum. The existence of a line at 33 ppm associated with the 2,1 erythro defect seems well supported in Figure 6 in the spectrum of the M327-0.42R2 iPP. This sample has negligible stereo defects; yet the resonance at 33 ppm is quite prominent in this sample relative to the other defect resonances. In contrast to the situation for the stereo-defect resonances, the situation presented in the difference spectrum of Figure 9 suggests no clear correspondence between defect intensities and defect concentration because all distinct defect resonances are not of equal intensity; i.e., the 33 ppm intensity is certainly smaller than the other defect intensities. Support for the idea that the 33 ppm line is weaker than the other defect resonances is not obvious in the spectrum of M327-0.42R2 in Figure 5, even though the stereo content of this sample is negligible. At the same time, the signal-to-noise ratio is not good enough to be convincing counter evidence that the 33 ppm line is weaker. Hence, we will assume that the 33 ppm line is indeed weaker than the other 2,1 erythro defect resonances.

The two resonances most easily integrated in the difference spectrum of Figure 9 are the lines at 35.3 ppm having intensity $0.21 \pm 0.03\%$ (where defect intensities are expressed as a percentage of each backbone resonance intensity in the middle spectrum of Figure 9). The methyl line at about 12 ppm has an intensity $0.22 \pm 0.07\%$. The larger uncertainty for the methyl integral is related to the broader resonance width and a greater uncertainty in the position of the baseline. Integration of the lines at 33 and 31.5 ppm is much more difficult and requires some assumption about the shape of the wings of the backbone resonances. Using the baselines indicated by the dashed lines in Figure 9 and the method of cutting and weighing yields respective integrals of the 33 and 31.5 ppm resonances equal to 0.11% and 0.30%. The integrals just mentioned are not similar to one another as was the case for the stereo-defect intensities. One possibility for obtaining resonances of about equal intensity is that the 35.3 ppm peak and the 33 ppm peak are multiplets belonging to the same carbon and that the 31.5 ppm peak corresponds to a second carbon. Finally, the 12 ppm peak, along with its shoulder at about 10 ppm, represents a third carbon, probably methyl, where the true baseline in the vicinity of this peak lies slightly below that indicated in Figure 9. In the foregoing scenario, each defect would give rise to three identifiable defect resonances such that, for the M236-1.17R2 sample, the concentration of defects in the CR region would be about 0.30% versus an overall concentration of 0.95%, thereby yielding a P_{CR}(2,1-erythro) of 0.32. On the other hand, if the integral at 35.3 ppm (and at 12 ppm with the baseline indicated in Figure 9) is a measure of the defect concentration in the CR region, then $P_{CR}(2,1\text{-erythro}) \approx 0.21/0.95 = 0.22$. Our lack of certainty about the assignment generates considerable ambiguity for these "P_{CR}" values. Our attempts to compute the spectrum of this defect in the lattice are described in a separate paper.[42] Agreement with experiment is not as good for the 2,1 erythro defect as it is for the stereo mrrm defect. Nevertheless, the smaller P_{CR} value suggested for the 2,1 erythro defect, relative to that of the mrrm stereo defect, stands in

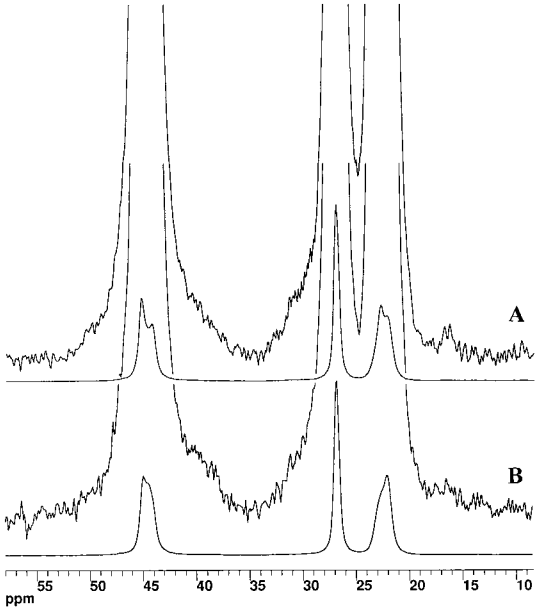

Figure 10. CR spectra of M9.8-2.80R3 samples with two different crystallization histories: slow cooling at 1 °C/min (lower spectrum) and solution crystallized (upper spectrum). Each spectrum is shown with vertical multiplication by ×1 and ×64. The latter sample is expected to contain only α-phase crystallites while the slowly cooled sample has mainly γ-phase crystallites. Note, despite the relatively high level of 1,3 defects, the absence of any distinct, narrow defect resonances suggesting (see text) that the 1,3 defect does not go into the CR region. The upfield wing of the main CH_2 resonance and the downfield wing of the main CH resonance are larger than in other samples, weakly suggesting that these defects may concentrate on the NC side of the interface.

contrast to other measures of the relative influence of stereo and regio defects. For example, in the promotion of γ-phase crystallinity, there is little distinction between the influence of stereo versus regio defects.[21]

We conclude our discussion of the incorporation of defects into the CR lattice of iPP by noting a few things about the spectrum of sample M9.8-2.80R3. This is the sample with an exceptionally low molecular mass (9.8 kg/mol) and an exceptionally high concentration of 1,3 defects (2.42%). None of the other samples had a concentration of 1,3 defects high enough to have any hopes of seeing observable resonances. In addition to the melt-crystallized sample which, according to Table 1, has crystallites which are 90% γ-phase, the as-received material was a powder precipitated from solvent. The latter process generally produces the α-phase. We looked at both samples. Both samples gave spectra with rather poor signal-to-noise because of lowered overall crystallinity; in addition, the spectrum of the latter sample had poorer signal-to-noise because the powder packed less well than the melt-crystallized sample.

Figure 10 shows the vertically amplified CR spectra of both samples of M9.8-2.80R3. Despite the high concentration of 1,3 defects, there are no distinct, relatively narrow defect resonances that can be identified. Hence, we conclude that there are no 1,3 defects which occupy well-defined positions in the CR lattice. The possibility that there could be many different allowed configurations near the 1,3 defect in the CR lattice (hence no sharp lines) we dismiss as improbable, even though a sequence of four methylene groups is quite flexible. The fact that the repeat unit associated with the 1,3 defect contributes three rather than two backbone carbons means that if such a defect is incorporated into the lattice, then the methyl groups that are either above or below the defect are one carbon out of position. Energetically this is costly. To avoid this, the configuration of such a defect demands that three backbone carbons occupy the space of two backbone carbons plus a branched methyl carbon in addition to presenting acceptable bond directions for continuing the chain in the lattice. While we intend to look into this problem in detail, our guess is that the geometric constraints seem difficult to satisfy; hence, for the present, we adopt the point of view that the absence of sharper defect resonances in Figure 10 indicates that the CR lattice fully rejects these 1,3 defects.

Two other observations are notable about the M9.8-2.80R3 sample. First, this is the only sample that showed significant contamination with some other organic material, possibly related to the catalyst. The experimental CP spectra possess a broad downfield shoulder with two broad maxima in the 60−80 ppm range. According to the high-resolution spectrum of the 1,3 defect,[11] no resonance has a significant shift downfield from the methylene backbone carbons. Thus, the large shifts observed are assigned to a contaminating species, which, incidentally, cannot be removed by reprecipitation from solution. The total intensity of the spurious resonances downfield from the iPP region corresponds to about 2.5% of the total iPP resonance intensity. Therefore, if we were to see any extra resonances within the iPP region, we would also have to prove that their origin is not the contaminating species. We seem to be fortunate in this regard because, in the separation of the CR from the NC signal, all evidence of this downfield intensity vanishes from the CR spectrum. Hence, there is good reason to expect that this contaminating material does not contribute to the CR spectrum in any spectral region.

The second observation regarding the M9.8-2.80R3 sample is that the upfield shoulder of the methylene resonance and the downfield shoulder of the methine resonance show slight excess intensity in the CR spectrum, relative to the shoulders of, say, the M327-0.42R2 sample. In the high-resolution spectrum, the four consecutive methylene carbons associated with the 1,3 defect resonate at about 28 and 38 ppm (two carbons at each position), and these shifts coincide reasonably well with the observed shoulders. In view of the higher concentration of the 1,3 defect in these materials and the effective doubling of the number of carbons contributing to each region, a possible interpretation for the shoulders is that these represent 1,3 defects on the NC side of the interface. Again, according to Figure 3, we expect some positive contribution from the NC side of the interface in the CR spectrum. The lack of sharpness of these resonances reinforces the idea that the environment for these defects is considerably disordered. The fact that the 1,3 defect contributes three flexible backbone carbons while requiring less volume than 1.5 isopropyl repeat units is a thermodynamic reason for attracting this defect to the interface. The interface is a region where topological issues clash with the constraints of available volume.[43] Albeit, owing to the helical backbone in CR iPP, this clash is not expected to be as strong in iPP as it is, for example, in an all-trans, chain-extended structure like polyethylene. The presence of the 1,3 defect with its reduced volume per

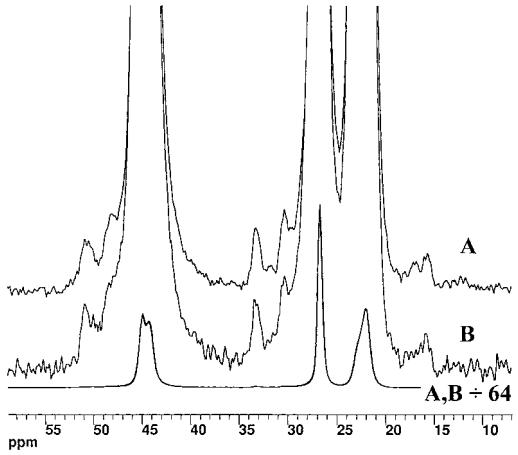

Figure 11. Comparison of CR spectra for M335-2.34S samples crystallized in two ways: top, cooling at 1 °C/min; middle, isothermal crystallization at 124 °C for 3 days; bottom, overlay of both upper spectra at a vertical amplification of (1/64). Stereo-defect intensities are comparable in both spectra despite the great difference in crystallization rates and although the fraction of γ-phase crystallites goes from about 0.5 (cooled) to about 0.8 (isothermal).

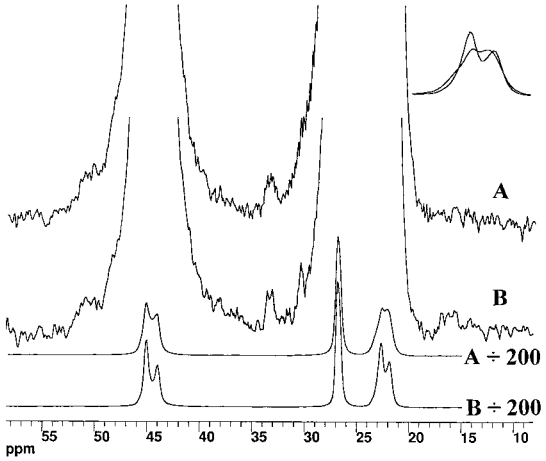

Figure 12. Comparison of CR spectra for Z250-0.9S samples crystallized in two ways: top, cooling at 1 °C/min; second, isothermal crystallization at 157 °C for 4 days; lower two plots are the same as those above (×1/200), and the small plot in upper right is an overlay of each methyl resonance. More highly resolved spectra are associated with the isothermally crystallized sample. Both samples crystallize exclusively into the α-phase; however, the changes in the line shape for the methyl carbon, changes which go beyond a simple improvement in resolution, support the claim by others that the α-phase exhibits different CR modifications; i.e., very slow crystallization does not simply improve the packing perfection of a single type of lattice. Within the signal-to-noise, stereo-defect intensities are comparable in both spectra despite slight changes in unit cell and despite the great difference in crystallization rates. NMR crystallinities increase by only 5% for the isothermally crystallized sample.

backbone length would reduce this problem. More work needs to be done, however, to confirm that the defects are indeed the origin of the additional shoulder intensities in this sample.

Finally, we wish to address briefly the question of whether the partitioning coefficients that have been claimed for these defects are strongly dependent on crystallization kinetics. We will cite only two observations, both relating to samples whose primary defect population is the stereo defect. In Figure 11 vertically amplified CR spectra of the M335-2.34S sample are

Table 3. Chemical Shifts and Relative Intensities for Identifiable Defect Resonances in iPP along with Partitioning Coefficients, P_{CR}(Defect), for Those Defects[a]

defect type	chemical shifts (ppm relative to TMS)	approx rel int[b]	P_{CR}[c]
stereo: mrrm	15.6(3) + 16.8(4)[d]	1.0(1)	0.48(6)[e] or 0.36(5)[f]
	30.1(3)	1.0(1)	
	33.1(2)	1.0(1)	
	47.9(4)	1.0(1)	
	50.6(3)	1.0(1)	
regio: 2,1 erythro	11.9(4) + 10.3(5)[d]	1.00(30)	0.32(6)[g] or 0.22(4)[h]
	31.6(3)	1.40(15)	
	33.1(4)	0.50(20)	
	35.3(3)	1.00(15)	
regio: 1,3	−	−	≈0

[a] The latter are based on the indicated assumptions. Standard uncertainties, expressed in units of the least significant digit, are indicated in parentheses. [b] These measures of relative intensities are based on the defect intensities for the corrected spectra shown in Figures 7 and 8 for the stereo and regio defects, respectively. [c] P_{CR} is defined as the ratio of defect concentration in the CR region to the sample-average defect concentration. [d] The second shift is that of a shoulder for the main defect-methyl resonance. [e] This P_{CR}(stereo) value uses the assumption that only the mrrm pentads contribute to the five observed resonances. [f] This P_{CR}(stereo) value uses the assumption (less likely, in our opinion) that all stereo defects, equal to half the mmmr concentration, contribute to the five observed resonances. [g] This P_{CR}(2,1-erythro) value uses the assumption that the 33.1 and 35.3 ppm "defect" peaks belong to the same carbon and the 31.6 ppm peak is another carbon. [h] This P_{CR}(2,1-erythro) value uses the assumption that the 11.9 and 35.3 ppm "defect" peaks belong to two different carbons. Also, the 33.1 ppm peak represents only about half the intensity of another carbon, where the resonance at 31.6 ppm represents the remaining intensity of that carbon plus another carbon.

compared. The top spectrum and middle spectrum correspond respectively to a sample cooled at 1 °C/min and a sample isothermally, melt-crystallized at 124 °C over a period of 3 days. This M335-2.34S sample had the highest concentration of stereo defects. The lower trace in Figure 11 is an overlay of both spectra, attenuated to 1/64. There is very little change in either the overall line shape or in the defect intensities as a result of the difference in crystallization kinetics. (The fraction of crystallites in the γ-phase is, however, changed from 0.5 to 0.6 to about 0.8 for the isothermally crystallized sample.[21]) Figure 12 shows vertically amplified CR spectra, representing melt crystallization at 1 °C/min (top) and isothermal crystallization at 157 °C for 4 days (bottom) for the Ziegler−Natta pseudofraction Z250-0.9S which crystallizes only into the α-phase for both crystallization conditions. Also shown are insets which overlay the backbone resonances for the methyl carbon, thereby illustrating that substantial changes in line shape occur as a result of slower crystallization. (Earlier[35] these changes in the shape of the methyl resonance were interpreted as evidence of substantial conversion from the α_1- to α_2-crystal form.) While the signal-to-noise ratio is not as good in Figure 12 as in Figure 11 for comparing defect intensities, within the signal-to-noise, the defect intensities for each of the spectra in Figure 12 are the same. Thus, in both of these cases, the defect concentration in the CR region remains approximately constant, whether crystallization takes place over days or over minutes, with changes in the α/γ ratio or with changes in the α_1/α_2 ratio. Thus, one might conclude that kinetics are not important. Recall, however, that all of our observations are made at

ambient temperature; hence, our observations are always subject to the criticism that, under very slow crystallization conditions, the defects are mainly incorporated into crystals which form during the cooling process. While we cannot completely dismiss this argument, it is not clear to us, supposing the very slow, isothermal crystallization completely rejected the defects, that all the rejected stems would be readily available for crystallization into those crystals formed upon cooling. Hence, our current bias is to think that the partitioning coefficients determined in this work and summarized in Table 3 for the stereo, 2,1-erythro and 1,3 defects have considerable generality.

On the basis of Figure 12, we also make one other inference. In the spectrum of the isothermally crystallized sample, one can discern all five defect-resonance regions for the stereo defect. Hence, these chemical shifts pertain to defects in the α-phase crystallites as well as to defects in the γ-phase crystallites, the latter being much more abundant in the M335-2.34S sample.

Conclusions

By employing solid-state ^{13}C NMR techniques, it has been shown that one can separate reasonably well the signals arising from the crystalline (CR) and the noncrystalline (NC) regions of isotactic polypropylene (iPP). Mainly metallocene-synthesized, melt-crystallized (at 1 °C/min cooling) iPP samples with varied, but known defect levels were studied. Different patterns of sharper, weak resonances, associated with different defects, can be distinguished from the backbone resonances in the spectra of the CR regions. These patterns of sharper resonances are associated with defects in highly ordered environments, not only on the basis of arguments from spin physics but also on the basis of the expectation that defects, incorporated into a highly ordered lattice, ought to adopt only one or two well-defined conformations with well-defined chemical shifts. It is also seen that the magnitudes of the chemical shift changes observed for stereo defects in a crystalline environment are much larger than the magnitudes of the corresponding changes in solution. The larger magnitudes in the solid state are associated with frozen conformations as opposed to highly averaged conformations in solution.

Simple stereo (mrrm-type) defects, typically the most abundant stereo-defect type in iPP's, are found to have a concentration in the CR regions of about half of their overall concentration provided the two following assumptions are correct: (a) each mrrm-type defect gives rise to five distinguishable defect resonances in the spectrum of the CR regions, and (b) "clustered" stereo defects, which involve departures from the ideal stereosequence, that extend over more than one monomer, do not contribute to the intensity of these five defect resonances. That five distinct resonances should be associated with each mrrm-type stereo defect is also borne out by the equal relative intensities of each defect resonance. For the two metallocene iPP's with dominant stereo defects, the concentration of defects in the CR region was found to be proportional to the overall concentration. However, for a Ziegler−Natta pseudofraction, the concentration of stereo defects in the CR region was a significantly lower fraction of the overall concentration than for the metallocene iPP's. This observation supports the claim of others that the Ziegler−Natta iPP chains possess a distribution, perhaps bimodal, of defect concentration per chain.

A resonance pattern associated with the regio 2,1 erythro defect was also identified. Four resonances were included in this pattern. However, the intensities of the individual defect resonances were not equal; hence, there is a more serious question about how many distinct resonances each defect produces. If one makes certain assumptions about this correspondence, then it is likely that the concentration of 2,1 erythro defects in the CR region lies somewhere between a quarter and a third of the sample-average defect concentration. In any case, the 2,1 erythro defect is more strongly discriminated against in the CR region than is the mrrm stereo defect.

Two other issues have been addressed briefly in this study. First, on the basis of spin diffusion modeling of the method for separating signals from the CR and NC regions, it is argued that the defects which are observed in the CR region are *not* highly concentrated at the CR/NC interface. Second, the fraction of the sample-average concentration of defects which is incorporated into the CR does not seem to depend strongly on crystallization kinetics or on the crystalline allomorph (α- or γ-crystallites).

We have also looked at partitioning in copolymers of iPP and 1-alkenes. A paper[43] dealing with ethylene copolymer defects has been submitted. We will report later on the copolymers involving longer 1-alkanes. Also, as mentioned in the text, we are very active in utilizing computational methods, both in the area of lattice energetics and in the area of chemical shift calculations in order to solidify the correspondence between each defect and the number of distinct resonances produced. The paper,[42] mentioned earlier, that describes these computations for the stereo-mrrm, the regio 2,1 erythro, the ethylene, and the butylene defects is in press.

Acknowledgment. The authors Dr. J. C. Randall of Exxon for stimulating and valuable discussions as well as assistance in the analysis of the high-resolution NMR data. We acknowledge Dr. Ernesto Pérez and Dr. Stefan Mansel of the Institute for Polymer Science and Technology in Madrid, Spain, for helpful discussions and for providing the M9.8-2.80R3 sample. R.G.A. acknowledges support of this work by the National Science Foundation, Polymer Program (DMR-9753258).

References and Notes

(1) Randall, J. C. *Polymer Sequence Determination: Carbon-13 NMR Method*; Academic Press: New York, 1977; Chapter 1.
(2) Isasi, J. R.; Mandelkern, L.; Galante, M. J.; Alamo, R. G. *J. Polym. Sci., Part B: Polym. Phys.* **1999**, *37*, 323.
(3) Cheng, S. Z. D.; Jnimak, J. J.; Zhang, A.; Hsieh, E. T. *Polymer* **1991**, *32*, 648.
(4) Cheng, S. Z. D.; Jnimak, J. J.; Zhang, A.; Hsieh, E. T. *Polymer* **1992**, *33*, 728.
(5) VanderHart, D. L.; Pérez, E. *Macromolecules* **1986**, *19*, 1902.
(6) Hartmann, S. R.; Hahn, E. L. *Phys. Rev.* **1962**, *128*, 2042.
(7) Brintzinger, H. H.; Fischer, D.; Mülhaupt, R.; Rieger, B.; Waymouth, R. M. *Angew. Chem., Int. Ed. Engl.* **1995**, *34*, 1143.
(8) Randall, J. C. *Macromolecules* **1997**, *30*, 803.
(9) Zambelli, A.; Locatelli, P.; Bajo, G.; Bovey, F. A. *Macromolecules* **1975**, *5*, 687.
(10) Hayashi, T.; Inoue, Y.; Chûjô, R.; Asakura, T. *Polymer* **1988**, *29*, 138.
(11) Soga, K.; Shiono, T. *Makromol. Chem. Rapid Commun.* **1987**, *8*, 305.
(12) Grassi, A.; Zambelli, A.; Resconi, L.; Albizzati, E.; Mazzocchi, R. *Macromolecules* **1988**, *21*, 617.

(13) Busico, V.; Cipullo, R.; Chadwick, J. C.; Modder, J. F.; Sudmeijer, O. *Macromolecules* **1994**, *27*, 7538.
(14) Belfiore, L. A.; Schilling, F. C.; Tonelli, A. E.; Lovinger, A.; Bovey, F. A. *Macromolecules* **1984**, *17*, 2561.
(15) Natta, G.; Corradini, P. *Suppl. Nuovo Cimento* **1960**, *15*, 40.
(16) Mencik, Z. *J. Makromol. Sci., Phys.* **1972**, *B6*, 101.
(17) Hikosaka, M.; Seto, T. *Polym. J.* **1973**, *5*, 111.
(18) Brückner, S.; Meille, S. V. *Nature* **1989**, *340*, 455.
(19) Meille, S. V.; Brückner, S.; Porzio, W. *Macromolecules* **1990**, *23*, 4114.
(20) Meille, S. V.; Ferro, D. R.; Brückner, S.; Lovinger, A. J.; Padden, F. J. *Macromolecules* **1994**, *27*, 2615.
(21) Alamo, R. G.; Kim, M.-H.; Galante, M. J.; Isasi, J. R.; Mandelkern, L. *Macromolecules* **1999**, *32*, 4050.
(22) Huang, M.-H.; Li, X.-G.; Fang, B.-R. *J. Apply. Polym. Sci.* **1995**, *56*, 1323. Li, J. X.; Cheung, W. L. *Polymer* **1999**, *40*, 2085.
(23) Brückner, S.; Meille, S. V.; Pettracone, V.; Pirozzi, B. *Prog. Polym. Sci.* **1991**, *16*, 361.
(24) Certain commercial companies are named in order to specify adequately the experimental procedure. This in no way implies endorsement or recommendation by the authors or their agencies.
(25) Lowe, I. J. *Phys. Rev. Lett.* **1959**, *2*, 85.
(26) Solomon, I. *C. R. Acad. Sci.* **1959**, *248*, 92.
(27) Saito, S.; Moteki, Y.; Nakagawa, M.; Horii, F.; Kitamaru, R. *Macromolecules* **1990**, *23*, 3256.
(28) VanderHart, D. L. *J. Magn. Reson.* **1987**, *72*, 13.
(29) Schaefer, J.; Stejskal, E. O.; Buchdahl, R. *Macromolecules* **1975**, *8*, 291.
(30) Abragam, A. *The Principles of Nuclear Magnetism*; Oxford University Press: New York, 1961; Chapter V.
(31) VanderHart, D. L.; McFadden, G. B. *Solid State Nucl. Magn. Reson.* **1996**, *7*, 45.
(32) Schmidt-Rohr, K.; Spiess, H. W. *Multidimensional Solid-State NMR and Polymers*; Academic Press: London, 1994; Chapter 13.
(33) Bunn, A.; Cudby, M. E. A.; Harris, R. K.; Packer, K. J.; Say, B. J. *Polymer* **1982**, *23*, 694.
(34) Brückner, S.; Meille, S. V.; Sozzani, P.; Torri, G. *Makromol. Chem. Rapid Commun.* **1990**, *11*, 55.
(35) Caldas, V.; Brown, G. R.; Nohr, R. S.; MacDonald, J. G. *J. Polym. Sci., Part B: Polym. Phys. Ed.* **1996**, *34*, 2085.
(36) Turner-Jones, A.; Aizlewood, J. M.; Beckett, D. R. *Makromol. Chem.* **1964**, *75*, 134.
(37) Caldas, V.; Morin, F. G.; Brown, G. R. *Magn. Reson. Chem.* **1994**, *32*, S72.
(38) Paukkeri, R.; Väänänen, T.; Lehtinen, A. *Polymer* **1993**, *34*, 2488.
(39) Paukkeri, R.; Lehtinen, A. *Polymer* **1994**, *35*, 1673.
(40) Xu, J.; Feng, L.; Yang, S.; Yang, Y.; Kong, X. *Eur. Polym. J.* **1998**, *34*, 431.
(41) Torchia, D. A. *J. Magn. Reson.* **1978**, *30*, 613.
(42) Nyden, M. R.; VanderHart, D. L.; Alamo, R. G. *Comput. Theor. Polym. Sci.*, in press.
(43) Guttman, C. M.; DiMarzio, E. A.; Hoffman, J. D. *Polymer* **1981**, *22*, 1466.
(44) Alamo, R. G.; VanderHart, D. L.; Nyden, M. R.; Mandelkern, L. *Macromolecules* **2000**, *33*, 6094.

MA992041P